

Physical Parameter Identification of Rheological Object Based on FE Dynamic Model

Z. K. Wang, S. Hirai
Dept. of Robotics, Ritsumeikan University
1-1-1 Noji Higashi
Kusatsu, Shiga 525-8577 JAPAN

Abstract - There are many kinds of deformable objects in our living life. Some of them demonstrate rheological behaviors during deformation, such as food, clay, human tissues, and organs. Usually, finite element (FE) model was employed to restructure or simulate the deformation behavior of such objects. However, there are important physical parameters to be known before simulation. In this paper, we presented an approach to estimate the physical parameters of rheological object based on FE dynamic model. Firstly, 1D FE dynamic model was described briefly and simulations were done with initial parameters. Secondly, the identification method was proposed according to analysis of deformation behavior and the identification results of simulation were given. Thirdly, this method was extended to 2D/3D deformation and experiment was done by using clay as rheological object. Finally, identification results of experiment were given and a new model for describing rheological deformation was proposed based on the curve fitting of force relaxation for experiment data.

I. INTRODUCTION

In surgical training and invasive surgery, precise simulations of human organs and tissues have to be done to describe and predict interaction between deformation and external forces or loads. Such simulation models have been intensively studied since late 80's and many methods had already been proposed to describe the deformation behavior of soft objects, such as: the mass-spring-damper method (MSD) [1], the finite difference method (FDM) [2], the boundary element method (BEM) [3], and the finite element method (FEM) [4]. The computation cost and force accuracy increase in this order. However, all of these models include important physical parameters which must be available before simulation. Unfortunately, there are little useful data can be obtained to describe these parameters until now.

In recent years, some methods had already been proposed to estimate such physical parameters for deformable objects. Most of them focus on elastic or viscoelastic deformation. One popular method is to iterate simulation with updated physical parameters. Material property is then obtained by minimizing the difference between displacements observed from images and calculated by simulations [5],[6],[7]. This method can take both nonlinear behavior and multi-layered structure into account and works well in dealing with elastic deformation with one or two unknown parameters, such as Young's modulus and Poisson's ratios. However, it is difficult to use this method in rheological deformation,

because rheological deformation includes viscous modulus which denotes the relationship between stress and velocity of strain. It is difficult to obtain the velocity of displacement during deformation in actual experiment. Another problem is local optimum. When we simulate deformation with more than one physical parameter, these parameters will interact with one another and contribute together to the final deformation. So, there can be more than one set of parameters that satisfy the final deformation during iterations.

So far, there are only few papers can be found working on parameter estimation for rheological deformation. Some of them employed MSD model to simulate and analyze the deformation of objects [8],[9],[10],[11]. But none of them took inner deformation into account. Our previous work had already developed an FE model for simulating rheological deformation [12]. In this paper, we proposed an approach to identify the physical parameters of rheological object based on this FE model.

II. FE DYNAMIC MODEL AND SIMULATION

A. 1D FE Dynamic Model

Depending on the deformation behavior in response to applied external force, deformable objects can be divided into three categories: viscoelastic, plastic, and rheological objects. Suppose that an object has a natural shape, as shown in Fig. 1(a). Applying external force, the object deformed as shown in Fig. 1(b). After external force is removed, viscoelastic objects return to the original shape and there is no residual deformation, as shown in Fig. 1(c). Plastic objects remain all the deformation and there is no recovered deformation, as shown in Fig. 1(d). However, rheological objects partially remain the deformation but not all, as shown in Fig. 1(e).

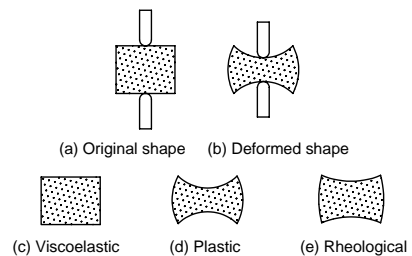


Figure 1. Deformation classification of soft objects

A. Identification for Long-time case

There are three unknown physical parameters in 1D rheological deformation: Young's modulus E , viscous modulus c_1 , and c_2 . We have to derive three equations to identify these parameters since there is only one set of force data can be obtained on the bottom.

1) *Force curve fitting in pull phase*: In three-element model, we have the relationship between stress σ and strain ε as follows [14]

$$\varepsilon = \varepsilon^{\text{voigt}} + \varepsilon^{\text{vis}}, \quad (2)$$

$$\sigma = E\varepsilon^{\text{voigt}} + c_1\dot{\varepsilon}^{\text{voigt}}, \quad (3)$$

$$\sigma = c_2\dot{\varepsilon}^{\text{vis}}, \quad (4)$$

By removing $\varepsilon^{\text{voigt}}$ and ε^{vis} , we have the following first order differential equation about stress and strain

$$\dot{\sigma} + \frac{E}{c_1 + c_2}\sigma = \frac{c_1c_2}{c_1 + c_2}\ddot{\varepsilon} + \frac{Ec_2}{c_1 + c_2}\dot{\varepsilon}. \quad (5)$$

In pull phase, $\dot{\varepsilon} = \text{constant}$ and $\ddot{\varepsilon} = \text{zero}$. We can obtain force approximation by solving above differential equation and replacing σ by \mathbf{F}_p , and ε by $\mathbf{J}\mathbf{u}_N$

$$\mathbf{F}_p(t) = c_2 \frac{\mathbf{J}\mathbf{u}_N^{\text{Keep}}}{t_p} + \left[\mathbf{F}_p(t_1) - c_2 \frac{\mathbf{J}\mathbf{u}_N^{\text{Keep}}}{t_p} \right] \exp\left(\frac{E}{c_1 + c_2}(t_1 - t)\right). \quad (6)$$

where $\mathbf{F}_p(t_1)$ is known force at time t_1 and $\mathbf{u}_N^{\text{Keep}}$ denotes displacements vector during keep phase. In Long-time simulation, vector $\mathbf{u}_N^{\text{Keep}}$ is equal to the final displacement vector $\mathbf{u}_N^{\text{Final}}$, as shown in Fig. 3(a).

2) *Force curve fitting in keep phase*: In keep phase, $\dot{\varepsilon} = 0$ and $\ddot{\varepsilon} = \text{zero}$. The force approximation in this phase can be obtained by solving (5)

$$\mathbf{F}_k(t) = \mathbf{F}_k(t_2) \exp\left(\frac{E}{c_1 + c_2}(t_2 - t)\right), \quad (7)$$

3) *Displacement transition*: In keep phase, displacement caused by elastic part totally turned into plastic part. So, we can obtain displacements of Voigt part at time t_p by integrating $\mathbf{F}_k(t)$ through t_p to infinite

$$\int_{t_p}^{\infty} \mathbf{F}_k(t) dt = \mathbf{F}_k(t_2) \int_{t_p}^{\infty} \exp\left(\frac{E}{c_1 + c_2}(t_2 - t)\right) dt = \frac{c_1 + c_2}{E} \mathbf{F}_k(t_p), \quad (8)$$

The velocity of Voigt part at time t_p can be obtained easily by using (2) and (4) and replacing σ by \mathbf{F}_p , ε by $\mathbf{J}\mathbf{u}_N$

$$\mathbf{J}\dot{\mathbf{u}}_N^{\text{Voigt}}(t_p) = \mathbf{J}\mathbf{u}_N^{\text{Keep}}/t_p - \mathbf{F}_p(t_p)/c_2, \quad (9)$$

Then, by substituting (8) and (9) into (3), we have

$$\mathbf{F}_p(t_p) - \mathbf{F}_k(t_p) = \left[c_1c_2/(c_1 + c_2) \right] \cdot \mathbf{J}\mathbf{u}_N^{\text{Keep}}/t_p. \quad (10)$$

Finally, we can identify unknown parameters in Long-time simulation by solving (6), (7) and (10). Identification results and errors were shown in Table II.

TABLE II
IDENTIFICATION RESULTS FOR LONG-TIME SIMULATION

Parameters	E (Pa)	c_1 (Pa·s)	c_2 (Pa·s)
Results	2.0006	8.0107	40.005
Error (%)	0.03	0.134	0.0125

B. Identification for Short-time case

In Short-time simulation, the rheological force does not decrease to zero during keep phase and displacements restore a little, i.e. $\mathbf{u}_N^{\text{Keep}} \neq \mathbf{u}_N^{\text{Final}}$. However, we assume that we only can obtain $\mathbf{u}_N^{\text{Final}}$ in actual experiment. So, we have to derive the relationship between $\mathbf{u}_N^{\text{Keep}}$ and $\mathbf{u}_N^{\text{Final}}$.

According to (3), the stress at time $(t_p + t_k)$ can be written as

$$\sigma(t_p + t_k) = E\varepsilon_{\text{Res}}^{\text{Voigt}} + c_1\dot{\varepsilon}^{\text{voigt}}(t_p + t_k), \quad (11)$$

where $\varepsilon_{\text{Res}}^{\text{Voigt}}$ denotes residual strain restored after releasing. During keep phase, the total strain keep constant, i.e. $\varepsilon^{\text{voigt}} + \varepsilon^{\text{vis}}$ is constant. By taking its time derivative, we have $\dot{\varepsilon}^{\text{voigt}} + \dot{\varepsilon}^{\text{vis}} = 0$. By substituting this into (11) and considering (4), we have

$$\varepsilon_{\text{Res}}^{\text{Voigt}} = \left[(c_1 + c_2)/(Ec_2) \right] \sigma(t_p + t_k), \quad (12)$$

At time $(t_p + t_k)$, we have

$$\varepsilon^{\text{Keep}} = \varepsilon^{\text{Final}} + \varepsilon_{\text{Res}}^{\text{Voigt}}, \quad (13)$$

By substituting (12) into (13), replacing σ by \mathbf{F}_k , and ε by $\mathbf{J}\mathbf{u}_N$, we can finally obtain the relationship between $\mathbf{u}_N^{\text{Keep}}$ and $\mathbf{u}_N^{\text{Final}}$

$$\mathbf{J}\mathbf{u}_N^{\text{Keep}} = \mathbf{J}\mathbf{u}_N^{\text{Final}} + \left[(c_1 + c_2)/(Ec_2) \right] \mathbf{F}_k(t_p + t_k). \quad (14)$$

Then, by substituting (14) into (6), we can obtain the first equation for force approximation of pull phase in Short-time simulation. The second equation for force approximation of keep phase is the same with (7). Now, let us derive the third equation about displacement transition in Short-time case. From Fig. 3(b) we know that the elastic displacements of Voigt model at time t_p partly translate into viscous displacement and residual elastic displacements recover after releasing. So, we can obtain the transition displacements at time t_p by integrating $\mathbf{F}_k(t)$ through time t_p to time $t_p + t_k$

$$\mathbf{J}\mathbf{u}_{\text{Tra}}^{\text{Voigt}} = \int_{t_p}^{t_p + t_k} \frac{\mathbf{F}_k(t)}{c_2} dt = \frac{c_1 + c_2}{Ec_2} \left[\mathbf{F}_k(t_p) - \mathbf{F}_k(t_p + t_k) \right], \quad (15)$$

The residual elastic displacements can be obtained by replacing σ by \mathbf{F}_k , and ε by $\mathbf{J}\mathbf{u}_N$ in (12). So, the total displacement of Voigt model at time t_p is

$$\mathbf{J}\mathbf{u}_N^{\text{Voigt}} = \mathbf{J}\mathbf{u}_{\text{Tra}}^{\text{Voigt}} + \mathbf{J}\mathbf{u}_{\text{Res}}^{\text{Voigt}} = \left[(c_1 + c_2)/(Ec_2) \right] \mathbf{F}_k(t_p), \quad (16)$$

Then, by substituting (9), (16) into (3) and considering (14), we can finally obtain the third equation as follows

$$\mathbf{F}_p(t_p) - \mathbf{F}_k(t_p) = \frac{c_1 c_2}{c_1 + c_2} \cdot \frac{\mathbf{J}_N^{\text{Final}}}{t_p} + \frac{c_1}{E} \cdot \frac{\mathbf{F}_k(t_p + t_k)}{t_p}. \quad (17)$$

Finally, we can identify unknown parameters in Short-time simulation by solving (6) with (14), (7) and (17). Identification results and errors were shown in Table III and curve fitting for both simulations are given in Fig. 4. Table III and Fig. 4 show the validity of this identification method for FE simulation. In next section, this will be extended to 2D/3D rheological deformation.

IV. 2D/3D RHEOLOGICAL DEFORMATION

A. FE Dynamic Model Extension

In 2D/3D isotropic elastic deformation, the relationship between stress and strain can be formulated as follows [13]:

$$\boldsymbol{\sigma} = (\lambda \mathbf{I}_\lambda + \mu \mathbf{I}_\mu) \boldsymbol{\varepsilon}, \quad (18)$$

where λ and μ denote Lamé's constants and matrices \mathbf{I}_λ and \mathbf{I}_μ originate from the isotropy of the object deformation.

In 2D/3D isotropic rheological deformation, we assume that deformation can be characterized by six parameters: λ^{ela} , μ^{ela} , λ_1^{vis} , μ_1^{vis} , λ_2^{vis} , and μ_2^{vis} . The first two are Lamé's constants, which describe elastic deformation. The next two describe viscosity and the last two show plasticity. For the sake of simplicity, we assume that these parameters are described by four physical parameters as below

$$\begin{aligned} \lambda^{\text{ela}} &= E \cdot \lambda^\gamma, & \lambda_1^{\text{vis}} &= c_1 \cdot \lambda^\gamma, & \lambda_2^{\text{vis}} &= c_2 \cdot \lambda^\gamma, \\ \mu^{\text{ela}} &= E \cdot \mu^\gamma, & \mu_1^{\text{vis}} &= c_1 \cdot \mu^\gamma, & \mu_2^{\text{vis}} &= c_2 \cdot \mu^\gamma, \end{aligned} \quad (19)$$

where $\lambda^\gamma = \gamma / [(1+\gamma)(1-2\gamma)]$ and $\mu^\gamma = 1 / [2(1+\gamma)]$.

TABLE III
IDENTIFICATION RESULTS FOR SHORT-TIME SIMULATION

Parameters	E (Pa)	c_1 (Pa·s)	c_2 (Pa·s)
Results	2.0046	8.0098	40.134
Error (%)	0.23	0.123	0.335

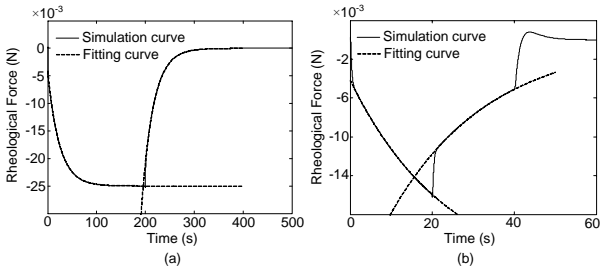


Figure 4. Comparison of the simulation data and fitting curves. (a) Curve fitting in Long-time simulation. (b) Curve fitting in Short-time simulation

Then, by solving (5) and replacing physical parameters by Lamé's constants given in (19), we can obtain the relationship between rheological force and displacement of 2D/3D deformation as follows

$$\mathbf{F} = \mathbf{J}_\lambda \boldsymbol{\Omega}_\lambda + \mathbf{J}_\mu \boldsymbol{\Omega}_\mu, \quad (20)$$

where \mathbf{J}_λ and \mathbf{J}_μ are two connection matrixes determined by geometric quantities, $\boldsymbol{\Omega}_\lambda$ and $\boldsymbol{\Omega}_\mu$ can be calculated as follows

$$\boldsymbol{\Omega}_\lambda = \Lambda^{\text{ela}} \lambda_2^{\text{vis}} \int_0^t \exp(-\Lambda^{\text{ela}}(t-t')) (\dot{\mathbf{u}}_N + \lambda_1^{\text{vis}} \dot{\mathbf{u}}_N / \lambda^{\text{ela}}) dt', \quad (21)$$

$$\boldsymbol{\Omega}_\mu = \Gamma^{\text{ela}} \mu_2^{\text{vis}} \int_0^t \exp(-\Gamma^{\text{ela}}(t-t')) (\dot{\mathbf{u}}_N + \mu_1^{\text{vis}} \dot{\mathbf{u}}_N / \mu^{\text{ela}}) dt',$$

where $\Lambda^{\text{ela}} = \lambda^{\text{ela}} / (\lambda_1^{\text{vis}} + \lambda_2^{\text{vis}})$, $\Gamma^{\text{ela}} = \mu^{\text{ela}} / (\mu_1^{\text{vis}} + \mu_2^{\text{vis}})$.

Finally, we can obtain the dynamic model of 2D/3D rheological deformation by replacing $\mathbf{J}\boldsymbol{\Omega}$ in (1) by \mathbf{F} in (20), vector \mathbf{a} and \mathbf{b} by corresponding matrices \mathbf{A} and \mathbf{B} , and $\boldsymbol{\Omega}$ by time derivative of (21).

B. Identification Method Extension

The identification equations in 2D/3D case can be easily obtained by extending the equations in 1D case. By replacing $c_2 \cdot \mathbf{J}$ in (6), (10), and (17) by $\lambda_2^{\text{vis}} \mathbf{J}_\lambda + \mu_2^{\text{vis}} \mathbf{J}_\mu$, replacing $E/(c_1+c_2)$ in (6) and (7) by $\lambda^{\text{ela}} / (\lambda_1^{\text{vis}} + \lambda_2^{\text{vis}})$, replacing $c_1/(c_1+c_2)$ in (10) and (17) by $\lambda_1^{\text{vis}} / (\lambda_1^{\text{vis}} + \lambda_2^{\text{vis}})$, and replacing c_1/E in (17) by $\lambda_1^{\text{vis}} / \lambda^{\text{ela}}$, we can finally obtain all the equations for identification of 2D/3D rheological deformation.

In 2D/3D rheological deformation, there are totally four unknown physical parameters: Young's modulus E , two viscous modulus c_1 , c_2 , and Poisson's ratio γ . But there are only three equations as presented above. However, it is noted that there are several nodal points on the bottom surface in 2D/3D deformation. We can employ the Least Square Method (LSM) among nodal points on the bottom surface of real object to solve above equations.

V. EXPERIMENT AND RESULTS

A. Pushing Experiment

The commercial clay made of flour, water, and salt was used as a rheological object through our experiments. The identification method given in Section III was employed to estimate the physical parameters. The clay of size 80mm×80mm×12.5mm was pushed by a motorized stage (made by SURUGA SEIKI Co.) with a displacement about 10mm and a constant velocity of 0.5mm/s. Before releasing, the displacement was kept about 48 seconds. Some markers were drawn on the surface of the clay by using a resist pen filled with lacquer ink. The deformation behaviors recorded by a camera are shown in Fig. 5(a), (b), and (c). By using a simple image processing, we can obtain a 2D FE mesh of these deformations as shown in Fig. 5(d), (e), and (f). The force data were recorded by a tactile sensor (made by NITTA Co.) as shown in Fig. 6. This sensor can measure the distribution of pressure.

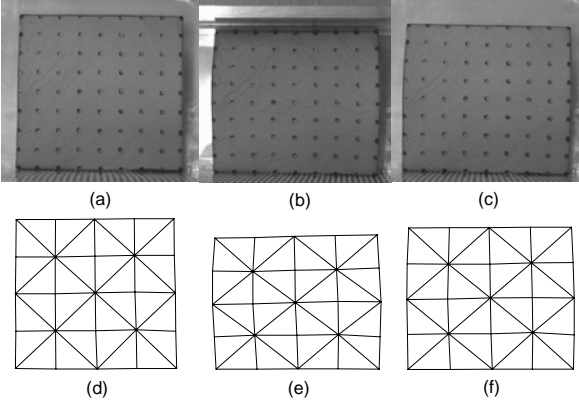


Fig. 5. Deformation behaviors in experiment: (a), (b), (c) Images taken by camera. (d), (e), (f) Description of images by using FE mesh. (a), (d) Initial shape. (b), (e) Deformed shape in the end of keep phase. (c), (f) Deformed shape in final condition.

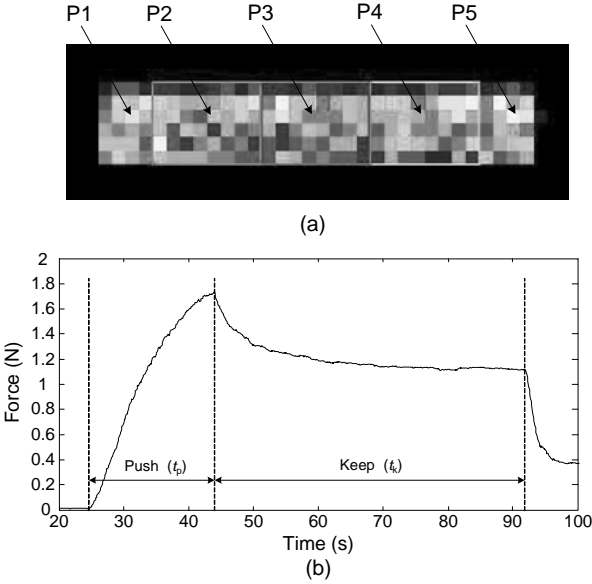


Fig. 6. Force response in experiment: (a) Force response in tactile sensor. (b) Force data on point P2.

B. Identification Results

As we assumed before, available data for us include the normal force at nodal points on the bottom surface and the final displacements of all nodal points. It is because the final displacements are easy to obtain in actual experiments and it can be calculated by subtracting the final position from the original position of nodal points.

Fig. 6(a) shows the pressure distribution on the bottom surface which was covered by 32×6 sensing elements. The bottom surface was divided into 5 segments. Each segment denotes one nodal point, as shown in Fig. 6(a). Three of them (P2, P3, and P4) include 8×6 sensing elements and the other two (P1 and P5) include 4×6 sensing elements. Force data

TABLE IV
IDENTIFICATION RESULTS

Parameters	E (Pa)	c_1 (Pa·s)	c_2 (Pa·s)	γ	Error (%)
Results	3.33×10^4	1.69×10^5	3.11×10^7	0.332	0.064

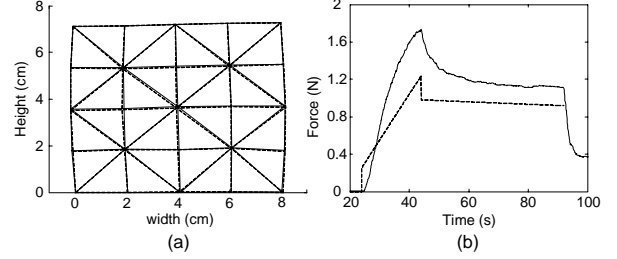


Fig. 7. Deformation comparison and force approximation: (a) Solid line denotes deformation in simulation using identified parameters and dashed line denotes deformation in real experiment. (b) Solid line shows force response in experiment and dashed line shows force results in simulation by using identified parameters.

acted on each point was calculated by summing up the force results of all sensing elements on corresponding segment. As shown in Fig. 6(b), the force data on point P2 did not decrease to zero after releasing. This is because the clay stuck to the sensor surface after releasing. We only use force data on nodal points P2, P3, and P4 in identification and the force data on P3 and P4 are quite similar with P2. The force data on P1 and P5 will not be used because we suppose the rheological force was concentrated in every nodal point in identification. However, P1 and P5 are on the boundary and only have half force data each in actual experiment.

By using the identification method presented in Section III and substituting displacement and force data into it, the physical parameters can be identified. Identification results are given in Table IV. Let $x_i^{\text{sim}}, y_i^{\text{sim}}, x_i^{\text{rel}},$ and y_i^{rel} be x and y coordinates of simulation and real deformation respectively, W and H be width and height of the object in the original shape. Then, the error was calculated by following equation

$$\text{Error} = \frac{\sum_{i=1}^{25} \left[\left(x_i^{\text{sim}} - x_i^{\text{rel}} \right)^2 + \left(y_i^{\text{sim}} - y_i^{\text{rel}} \right)^2 \right]}{W \times H} \times 100 \quad [\%]$$

The deformation difference between simulation and experiment at the end of keep phase is quite small as shown in Fig. 7(a) and Table IV. In contrary, Fig. 7(b) shows that we cannot obtain a good approximation of the force even though the deformations are almost the same. This is because the three-element model used in this paper is a linear model. Rheological objects in the real world demonstrate many nonlinear behaviors. However, if we only focus on the deformation behavior when the object is subject to displacement constraint and the accuracy of force response is not important, we still can use this model to simulate the rheological deformation.

C. Discussion on the Force Relaxation

As shown in Fig. 6(b), during the keep phase, the rheological response of force relaxation is dominant. In three-element model, this force response can be described by one exponential decay function, as given in (7). However, experiment result shows that one exponential decay function can not obtain a good curve fitting for the force relaxation. Reference [15] stated that we can choose two exponential terms to approximate the relaxation behavior. According to (7), we choose follow equation to approximate the force relaxation in the keep phase

$$F(t) = A \cdot \exp(-a(t-t_1)) + B \cdot \exp(-b(t-t_1)), \quad (22)$$

when $A=0.3879$, $B=1.1975$, $a=0.22$, and $b=0.0015$, we can obtain a good curve fitting for the experiment data, as shown in Fig. 8(a). This means that there must be at least two exponential functions in (7) during the keep phase. Based on this consideration, let us change the three-element model to a new model which include one Maxwell models connected with a viscous element in parallel and another elastic element, as shown in Fig. 8(b).

In this model, we can easily obtain the relationship between stress and strain as follows

$$\ddot{\sigma} + A_1 \dot{\sigma} + A_2 \sigma = B_1 \ddot{\varepsilon} + B_2 \dot{\varepsilon}, \quad (23)$$

where

$$A_1 = \frac{E_2 c_1 + E_1 (c_1 + c_2)}{c_1 c_2},$$

$$A_2 = \frac{E_1 E_2}{c_1 c_2},$$

$$B_1 = E_2,$$

$$B_2 = \frac{E_1 E_2 (c_1 + c_2)}{c_1 c_2}.$$

During the keep phase, the total strain keeps a constant, i.e. $\dot{\varepsilon} = 0$ and $\ddot{\varepsilon} = 0$. Thus, we can obtain the analytical expression of force relaxation in this phase by solving (23)

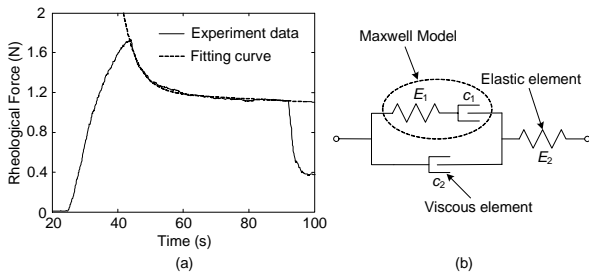


Fig. 8. Curve fitting for experiment data and a new model: (a) Solid line denotes force data in actual experiment and dashed line denotes curve fitting by using two exponential decay functions. (b) A new model with two Maxwell models connected in parallel and another elastic element.

$$\sigma(t) = P \cdot \exp(-m(t-t_1)) + Q \cdot \exp(-n(t-t_1)), \quad (24)$$

where

$$P = \frac{\sqrt{A_1^2 - 4A_2} - A_1}{2\sqrt{A_1^2 - 4A_2}} \sigma(t_1) - \frac{1}{\sqrt{A_1^2 - 4A_2}} \cdot \dot{\sigma}(t_1),$$

$$Q = \frac{\sqrt{A_1^2 - 4A_2} + A_1}{2\sqrt{A_1^2 - 4A_2}} \sigma(t_1) + \frac{1}{\sqrt{A_1^2 - 4A_2}} \cdot \dot{\sigma}(t_1),$$

$$m = \frac{A_1 + \sqrt{A_1^2 - 4A_2}}{2},$$

$$n = \frac{A_1 - \sqrt{A_1^2 - 4A_2}}{2},$$

$\sigma(t_1)$ is a integral initial value at time t_1 which should be close to the starting time of keep phase.

By comparing (24) with (22), we found that the model shown in Fig. 8(b) is better than three-element model to describe rheological deformation. We can obtain a good approximation of force relaxation during the keep phase.

VI. CONCLUSION AND FUTURE WORKS

In this paper, an identification method of physical parameters for rheological deformation based on a FE dynamic model was presented. Since this method only involved theoretical analysis and simple calculation, it is easy and fast to identify the parameters when the required data are available. The required data used in this method include the force data of some nodal points on the bottom or the top surface which can be measured by a tactile sensor and the final displacements of all nodal points which can be obtained by using a camera in 2D deformation and a CT or MRI device in 3D case. Experiment results show that by using the three-element model we can not obtain a good force approximation. Based on curve fitting of force relaxation, we proposed a new model which includes one Maxwell model connected with a viscous element in parallel and another elastic element. We believe this model can be employed to describe rheological deformation and it is better than three-element model. In addition, this identification method presented in this paper also can be used in elastic or viscoelastic deformation.

In our future works, the new model will be applied to 2D/3D FE dynamic model to simulate rheological deformation and the identification method of physical parameter will be developed based on this model. Moreover, the new model and the identification method will be extended to non-uniform rheological deformation.

REFERENCES

- [1] K. Waters, "A muscle model for animating three-dimensional facial expression," in *Proc. of the 14th Annual Conference on Computer Graphics and Interactive Techniques*, Anaheim, 1987, pp. 17-24.
- [2] D. Terzopoulos, J. Platt, A. Barr, K. Fleischer, "Elastically deformable models," in *Proc. of the 14th Annual Conference on Computer Graphics and Interactive Techniques*, Anaheim, 1987, pp. 205-214.

- [3] D. L. James, D. K. Pai, "Artdefo: accurate real time deformable objects," in *Proc. of the 26th Annual Conference on Computer Graphics and Interactive Techniques*, Los Angeles, 1999, pp. 65-72.
- [4] M. B. Nielsen, S. Cotin, "Real-time volumetric deformable models for surgery simulation using finite elements and condensation," in *Computer Graphics Forum (Proc. Eurographics '96)*, Poitiers, 1996, pp. 57-66.
- [5] M. Tada, N. Nagai, T. Maeno, "Material properties estimation of layered soft tissue based on MR observation and iterative FE simulation," in *Medical Image Computing and Computer-Assisted Intervention*, vol. 3750, Springer Berlin/Heidelberg, 2005, pp. 633-640.
- [6] T. Hoshi, Y. Kobayashi, K. Kawamura, M. G. Fujie, "Developing an intra-operative methodology using the finite element method and the Extended Kalman filter to identify the material parameters of an organ model," in *Proc. of the 29th Annual International Conference of the IEEE EMBS*, Lyon, 2007, pp. 469-474.
- [7] T. Hoshi, Y. Kobayashi, M. G. Fujie, "Developing a method using the Extended Kalman Filter to identify the material parameters of deformation model of organ," in *Proc of the 2008 JSME Conference on Robotics and Mechatronics*, Nagano, 2008, pp. 1A1-C18.
- [8] N. Ueda, S. Hirai, H. T. Tanaka, "Extracting rheological properties of deformable objects with haptic vision," in *Proc. of the 2004 IEEE International Conference on Robotics and Automation*, New Orleans, 2004, pp. 3902-3907.
- [9] H. Noborio, R. Enoki, S. Nishimoto, T. Tanemura, "On the calibration of deformation model of rheology object by a modified randomized algorithm," in *Proc. of the 2003 IEEE International Conference on Robotics and Automation*, Taipei, 2003, pp. 3729-3736.
- [10] R. Nogami, H. Noborio, F. Ujibe, H. Fujii, "Precise deformation of rheologic object under MSD models with many voxels and calibrating parameters," in *Proc. of the 2004 IEEE International Conference on Robotics and Automation*, New Orleans, 2004, pp. 1919-1926.
- [11] H. Yoshida, Y. Murata, H. Noborio, "A smart rheologic MSD model pushed/calibrated/evaluated by experimental impulses," in *IEEE/RSJ International Conference on Intelligent Robots and Systems (IROS 2005)*, Edmonton, 2005, pp. 269-276.
- [12] J. Muramatsu, T. Ikuta, S. Hirai, "Validation of FE deformation models using ultrasonic and MR images," in *Proc. of the 9th International Conference on Control, Automation, Robotics and Vision*, Singapore, 2006, pp. 1-6.
- [13] I. H. Shames, F. A. Cozzarelli, *Elastic and Inelastic Stress Analysis*. New Jersey: Englewood, 1992, ch. 4.
- [14] S. Hirai, S. Tomokuni, "Dynamic modeling of rheological deformation," *JSME Conf. on Robotics and Mechatronics Division*, 2004, 2A1-H-7.
- [15] C. D. Tsai, I. Kao, "Applying viscoelastic contact modeling to grasping task: an experimental case study," in *Proc. of the 2008 IEEE/RSJ International Conference on Intelligent Robots and System*, Nice, 2008, pp. 1790-1795.